Probing the mechanism of improved performance for sodium-ion batteries by utilizing three-electrode cells: Effects of sodium-ion concentration in ionic liquid electrolytes

Takayuki YAMAMOTO,[1,*] Kazushi MITSUHASHI,[2] Kazuhiko MATSUMOTO,[2] Rika HAGIWARA,[2] Atsushi FUKUNAGA,[3] Shoichiro SAKAI,[3] Koji NITTA,[3] and Toshiyuki NOHIRA[1,*]

[1] Institute of Advanced Energy, Kyoto University, Gokasho, Uji 611-0011, Japan

[2] Graduate School of Energy Science, Kyoto University, Yoshida-honmachi, Sakyo-ku, Kyoto 606-8501, Japan

[3] Sumitomo Electric Industries, Ltd., 1-1-3 Shimaya, Konohana-ku, Osaka 554-0024, Japan

[*] Corresponding Authors:

*E-mail: yamamoto.takayuki.2w@kyoto-u.ac.jp, Tel: +81-774-38-3498, Fax: +81-774-38-3499 (T.Y.).

*E-mail: nohira.toshiyuki.8r@kyoto-u.ac.jp, Tel: +81-774-38-3500, Fax: +81-774-38-3499 (T.N.).

Abstract

We investigated the full-cell performance of sodium-ion batteries composed of a hard carbon (HC) negative electrode, a $NaCrO_2$ positive electrode, and an ionic liquid electrolyte Na[FSA]–[C_3C_1pyrr][FSA] (FSA = bis(fluorosulfonyl)amide, C_3C_1pyrr = *N*-methyl-*N*-propylpyrrolidinium) at 333 K. Before the full-cell tests, charge–discharge tests of the Na/HC and Na/$NaCrO_2$ half cells were conducted, from which the practical capacities were determined to be ca. 250 mAh $(\text{g-HC})^{-1}$ and ca. 115 mAh $(\text{g-}NaCrO_2)^{-1}$, respectively. Using these capacities, the performance of HC/$NaCrO_2$ full cells with practical loading masses was evaluated by three-electrode cells with a sodium metal reference electrode, and the energy density was calculated to be 177 Wh $(\text{kg-}(NaCrO_2 + \text{HC}))^{-1}$. In particular, we focused on the effect of the sodium-ion concentration on the performance by varying the molar fraction of Na[FSA] (x(Na[FSA])) from 0.20 to 0.50. The best rate capability was obtained at a composition of x(Na[FSA]) = 0.50. The effect of the sodium-ion concentration was discussed in terms of the potential profiles of the positive and negative electrodes. The results were explained by the sodium-ion supplying capability of the electrolyte inside the electrode, where the sodium insertion reaction occurs.

Keywords: Sodium-ion battery, Ionic liquid, High concentration, Full-cell performance

1. Introduction

Lithium-ion batteries (Li-ion batteries; LIBs) have become widespread in small electronic devices such as mobile phones and PC laptops due to their high energy densities. Recently, many researchers and companies have struggled to develop large-scale LIBs, especially for electric vehicles and stationary storage batteries.[1,2] Two issues have emerged as the main concerns with the adoption of such large-scale electrical energy storage systems. One issue is safety, due to the utilization of flammable organic solvent-based electrolytes. In general, the specific surface area per volume decreases with increasing size, and thus large batteries inherently face difficulties in releasing heat to the environment, which can lead to thermal runaway and result in ignition accidents. Based on the backgrounds, ionic liquids are promising electrolytes, owing to their high safety in terms of non-flammability and negligible volatility. In recent decades, intensive studies on the development of ionic liquid electrolytes for LIBs have been conducted.[3–5]

Another problem is the scarcity of lithium and cobalt resources, which are used in the main components of current LIBs; it will not be possible to meet the demand for these resources in the production of large-scale power storage devices in the future.[6–8] Thus, new batteries utilizing more abundant resources that represent feasible alternatives to LIBs must be developed. Sodium-ion batteries (Na-ion batteries; NIBs) are promising candidates for large-scale applications because sodium resources are abundant in the earth's crust and sea water.[9,10] Moreover, although copper current collectors are needed for the negative electrodes in LIBs, inexpensive aluminum current collectors can be used for both the negative and positive electrodes in NIBs.

Recently, several groups have reported the full-cell performance of organic solvent-based NIBs,[11–13] some of which have shown energy densities higher than 200 Wh kg^{-1} based on the total mass of active materials in the positive and negative electrodes. However, most of these NIBs utilized a loading mass lower than 10 (mg-positive active materials) cm^{-2}, and almost no intensive studies on practical-scale NIBs have been conducted.

Many researchers have reported a variety of active materials and electrolytes for NIBs, and several groups, including ours, have focused on developing ionic liquid electrolytes that fulfill both safety and performance requirements.[14–30] Our group has developed the ionic liquid Na[FSA]–[C_3C_1pyrr][FSA] (FSA = bis(fluorosulfonyl)amide, C_3C_1pyrr = *N*-methyl-*N*-propylpyrrolidinium), and found that the composition of *x*(Na[FSA]) = 0.20 (*x*(Na[FSA]) = molar fraction of Na[FSA]) exhibited a reasonably high ionic conductivity of 3.6 mS cm^{-1} and a wide electrochemical window of ca. 5 V at 298 K.[24] The standard redox potential of Na^+/Na in water is higher than that of Li^+/Li by 0.3 V, which decreases the energy densities of NIBs. However, the potential differences between these redox couples depend on the electrolyte. For example, in the case of the ionic liquid electrolyte M[FSA]–[C_3C_1pyrr][FSA] (M = Li, Na; *x*(M[FSA]) = 0.20), the potential difference is reduced to ca. 0.1 V ($E(Na^+/Na) \approx E(Li^+/Li) + 0.1$).[31] Thus, the utilization of ionic liquid electrolytes can eliminate the drawback of reduced energy density for NIBs. In addition, one of the most unique characteristics for ionic liquid batteries is the wide operating temperature range, which realizes superior performance at intermediate temperature range (333–363 K) compared with room temperature, due to their higher ionic conductivities as well as higher reactivity of the electrode materials.

We have shown that a variety of active materials can be used in the ionic liquid

Na[FSA]–[C_3C_1pyrr][FSA].[25–27] Very recently, we realized a practical sodium-ion full cell consisting of a hard carbon (HC) negative electrode and a $NaCrO_2$ positive electrode, which reached energy densities of 125 Wh L^{-1} and 75 Wh kg^{-1} at an operating temperature range of 298–363 K.[28] However, the sodium-ion concentration of the ionic liquid electrolyte was as low as 1 mol dm^{-3}, and there is room to improve the performance by increasing the composition of Na[FSA]. In fact, the $NaCrO_2$ positive electrode shows better rate capability at a composition of x(Na[FSA]) = 0.40 or 0.50.[29]

In the present study, we investigated the performance of HC/Na[FSA]–[C_3C_1pyrr][FSA]/$NaCrO_2$ full cells utilizing practical loading masses of 4.8–6.9 (mg-HC) cm^{-2} and 12.3–15.4 (mg-$NaCrO_2$) cm^{-2}. We adopted the three-electrode cell configuration with a sodium metal reference electrode in order to evaluate the charge–discharge behaviors of both the positive and negative electrodes separately, and discussed the effect of the sodium-ion concentration on the rate capability of the sodium-ion full cells in the ionic liquids Na[FSA]–[C_3C_1pyrr][FSA] (x(Na[FSA]) = 0.20–0.50) at 333 K.

2. Experimental

2.1 Reagents and their handling

Na[FSA] (>99+%; Mitsubishi Materials Electronic Chemicals Co., Ltd.) and [C_3C_1pyrr][FSA] (>99.9%; Kanto Chemical Co., Inc.) were dried under vacuum prior to use. The drying temperature and time were respectively 353 K and 48 h for Na[FSA], and 333 K and 24 h for [C_3C_1pyrr][FSA]. The Na[FSA]–[C_3C_1pyrr][FSA] ionic liquids (x(Na[FSA]) = 0.20, 0.30, 0.40, and 0.50) were prepared by mixing Na[FSA] and [C_3C_1pyrr][FSA] in an argon-filled glove box. The sodium-ion concentrations for all the

compositions are summarized in Table S1.

The preparation procedures for the hard carbon (HC) and $NaCrO_2$ electrodes were as follows. An aqueous slurry was prepared by mixing HC powder (CARBOTRON P, Kureha Battery Materials Japan Co., Ltd), carboxymethyl cellulose (CMC), and styrene-butadiene rubber (SBR) in a weight ratio of HC/CMC/SBR = 97/2/1. Similarly, $NaCrO_2$ powder, acetylene black (AB), and polyvinylidene difluoride (PVdF) were mixed in *N*-methyl-2-pyrrolidone (NMP) with a weight ratio of $NaCrO_2$/AB/PVdF = 92/5/3 to make a slurry. $NaCrO_2$ was synthesized by the solid-state reaction method which was reported previously.[25] Both slurries were coated onto aluminum foils, and were dried at 363 K in air to remove the solvents. Finally, these electrodes were dried under vacuum at 423 K for 24 h. The loading masses of HC and $NaCrO_2$ were within the ranges of 4.8–6.9 mg cm^{-2} and 12.3–15.4 mg cm^{-2}, respectively.

2.2 Charge–discharge tests and analysis

2.2.1 Two-electrode half cells

Charge–discharge tests were conducted using electrochemical measurement apparatuses (VSP, Bio-Logic Co., or 580-type battery cycler, Toyo Co.). The charge–discharge behaviors of a HC electrode and a $NaCrO_2$ electrode were investigated respectively using 2032-type coin cells under an argon atmosphere. The working electrode was a HC or $NaCrO_2$ electrode, and the counter electrode was sodium metal. The Na[FSA]–[C_3C_1pyrr][FSA] ionic liquids (x(Na[FSA]) = 0.20, 0.30, 0.40, and 0.50) were used as the electrolyte. Both the HC and $NaCrO_2$ electrodes were impregnated with the electrolytes under vacuum before assembling the cells. The operating voltage ranges were 0.005–1.4 V for the Na/HC half cell, and 2.5–3.5 V for the Na/$NaCrO_2$ half

cell. The operating temperatures were set to 313 or 353 K. The charge–discharge rates are provided in the section of Results and discussion.

2.2.2 Three-electrode full cell

A sodium-ion full cell was constructed using an air-tight three-electrode cell (Hohsen Corp.; see Figure S1) in the argon-filled glovebox. A two-ply polyolefin filter (50 μm thickness per sheet) was used as a separator. The HC negative electrodes, $NaCrO_2$ positive electrodes, and polyolefin filters were vacuum-impregnated with the electrolyte prior to the test. Sodium metal was used as a reference electrode. The temperature of the three-electrode cell was controlled using a temperature-controlled bath. Based on the results of the half-cell tests, the practical capacities of HC and $NaCrO_2$ were assumed to be 250 and 115 mAh g^{-1}, respectively. In the sodium-ion full cells, the ratio of the practical capacities of HC and $NaCrO_2$ (N/P ratio; $R_{N/P}= Q_{HC}/Q_{NaCrO_2}$: Q is the quantity of electricity (C)) were controlled to be within the range of 0.85–1.00. The loading masses and N/P ratios of HC/$NaCrO_2$ full-cells for discharge and charge rate capability tests are summarized in Tables S2 and S3, respectively. For the current densities, in this study, a rate of 100 mA $(g\text{-}NaCrO_2)^{-1}$ was regarded as 1C rate. The cut-off potentials were set at 0.002 and 1.5 V (vs. Na^+/Na) for the HC negative electrodes, and 2.5 and 3.5 V (vs. Na^+/Na) for the $NaCrO_2$ positive electrodes. The cut-off voltages were 1.5 and 3.4 V for the full cells. When the potentials and voltages reached at least one of these limits, the system was switched from charging to discharging or vice versa.

The operating procedures were as follows. First, to stabilize the performance of the sodium-ion cells, all the full-cells were operated at 0.2C rate for 3 cycles with the

charge capacity limited to 85 mAh (g-$NaCrO_2$)$^{-1}$, and then operated at 0.2C rate without the capacity limitation for an additional 5 cycles. This stabilization step was conducted at 313 K (x(Na[FSA]) = 0.20, 0.30, 0.40) or 333 K (x(Na[FSA]) = 0.50). For all the full cells, the subsequent rate capability tests were performed at 333 K. In the discharge rate capability test, the charge rate was fixed at 0.5C, and various discharge rates were tested from the lowest (0.5C) to the highest (8C). A similar procedure was adopted for the charge rate capability test.

2.2.3 Instrumental analysis

The surface morphologies and the elemental distributions of a HC electrode and a $NaCrO_2$ electrode were observed using a field emission scanning electron microscope (FE-SEM; SU-8020, Hitachi) and with an energy dispersive X-ray spectrometer (EDX; X-max, Horiba, or X-max^{N}80, Oxford Instruments).

3. Results and discussion

3.1 Charge–discharge behavior of the Na/HC and Na/$NaCrO_2$ half cells

Figure 1 shows selected surface SEM images of the HC and $NaCrO_2$ electrodes. The size distributions of the HC and $NaCrO_2$ particles were confirmed to be 2–10 μm and 1–2 μm, respectively. In addition, selected results of the SEM observations and EDX mapping analysis for both electrodes are summarized in Figure S2. For the HC electrode (Figure S2a–S2c), carbon and sodium are detected by EDX mapping. The carbon-rich areas correspond to the HC particles according to the SEM results, and sodium is detected over the whole electrode surface. Since CMC is the only source of sodium in the HC electrode, this result indicates that the CMC binder is homogeneously

dispersed in the HC electrode. On the other hand, for the $NaCrO_2$ electrode (Figure S2d–S2h), the carbon component is attributed to the conductive agent (acetylene black), and the sodium and chromium are ascribed to the $NaCrO_2$ particles. Fluorine is detected on the whole area of the electrode surface. Since the PVdF binder is the only the fluorine source, this indicates that the binder is almost uniformly distributed in both the electrode composite.

Figure 2 shows the typical charge–discharge performance of the HC and $NaCrO_2$ electrodes using two-electrode half cells with sodium metal counter electrodes. As shown in Figure 2a, the discharge capacities obtained for the HC electrode at 313 and 353 K are 230 and 256 mAh $(g\text{-HC})^{-1}$, respectively. The first three cycles were measured at 313 K, while the subsequent three cycles are conducted at 353 K, as shown in Figure 2b. Higher capacities are observed at 353 K due to the extension of the plateau region at around 0.1 V. This mainly originates from the lower resistance for sodium-ion diffusion in the surface layer of the sodium metal counter electrode at higher temperatures.[26] Based on the above results, a capacity of 250 mAh $(g\text{-HC})^{-1}$ is adopted as the standard practical capacity of HC for the calculation of the N/P ratios in the HC/$NaCrO_2$ full cells. As shown in Figure 2c and 2d, the $NaCrO_2$ electrode shows a stable reversible capacity of approximately 115 mAh $(g\text{-}NaCrO_2)^{-1}$ at both 313 and 353 K. Thus, the standard practical capacity of $NaCrO_2$ is determined to be 115 mAh $(g\text{-}NaCrO_2)^{-1}$.

3.2 Charge–discharge behavior of the HC/$NaCrO_2$ full cell

Figure 3 shows typical charge–discharge curves of the HC/$NaCrO_2$ three-electrode full cell with an electrolyte composition of x(Na[FSA]) = 0.20. The solid line, the

broken line, and the dotted line correspond to the cell voltage, the potential of the $NaCrO_2$ positive electrode, and the potential of the HC negative electrode, respectively. The charge–discharge profiles of HC and $NaCrO_2$ are consistent with the above results from the two-electrode half cells, which indicates that the sodium-ion full cell functions properly.

A reversible capacity of 92 mAh (g-$NaCrO_2$)$^{-1}$ is obtained at a rate of 0.5C. Since the N/P ratio, $R_{N/P}$, of this cell is 0.88, the ideal practical capacity of the cell is calculated to be 101 mAh (g-$NaCrO_2$)$^{-1}$ using Eq. (1).

$$C^{\mathrm{Id}}_{\text{Full-cell (NaCrO}_2\text{)}} = C^{\mathrm{Std}}_{\mathrm{NaCrO_2}} \times R_{\mathrm{N/P}} \qquad (R_{\mathrm{N/P}} \leq 1) \tag{1}$$

where $C^{\mathrm{Id}}_{\text{Full-cell (NaCrO}_2\text{)}}$ is the ideal practical capacity of the full cell and $C^{\mathrm{Std}}_{\mathrm{NaCrO_2}}$ is the standard practical capacity of $NaCrO_2$ (115 mAh (g-$NaCrO_2$)$^{-1}$). Thus, the full cell has achieved almost 90% of the ideal practical capacity. The deviation between the ideal and obtained full-cell capacities can be explained by the irreversible capacity of the hard carbon negative electrode (ca. 40 mAh (g-HC)$^{-1}$). The average operating voltage during discharge (V_{Average}) of this full cell is calculated by the following Eq. (2).

$$V_{\mathrm{Average}} = \left(\int_0^{Q_{\mathrm{d}}} V \,\mathrm{d}Q\right) / Q_{\mathrm{d}} \tag{2}$$

where V is the cell voltage and Q_{d}(C) is the total quantity of charge during discharge process. In this case, V_{Average} is calculated to be 2.72 V. The gravimetric energy density of the full cell, $W_{\text{Full-cell}}$ (mWh g^{-1} = Wh kg^{-1}), is defined as:

$$W_{\text{Full-cell}} = \frac{V_{\mathrm{Average}} \times (Q_{\mathrm{d}}/3.6)}{m_{\mathrm{NaCrO_2}} + m_{\mathrm{HC}}} \tag{3}$$

where $m_{\mathrm{NaCrO_2}}$(g) and m_{HC}(g) are the weight of $NaCrO_2$ and HC, respectively. It should be noted that 1 mAh = 3.6 C. Here, $W_{\text{Full-cell}}$ can also be calculated from specific capacities of $NaCrO_2$ and HC as follows.

The specific capacities of $NaCrO_2$ and HC, C_{NaCrO_2} (mAh (g-$NaCrO_2$)$^{-1}$) and C_{HC} (mAh (g-HC)$^{-1}$), are expressed as

$$C_{NaCrO_2} = \frac{Q_d/3.6}{m_{NaCrO_2}} \quad (4)$$

$$C_{HC} = \frac{Q_d/3.6}{m_{HC}} \quad (5)$$

Then, from Eqs. (3), (4) and (5), the gravimetric energy density, $W_{Full\text{-}cell}$ (Wh (kg-($NaCrO_2$ + HC))$^{-1}$), is obtained by the following equation;

$$W_{Full\text{-}cell} = V_{Average} \times \frac{C_{NaCrO_2} \times C_{HC}}{C_{NaCrO_2} + C_{HC}} \quad (6)$$

In the case of the discharge curve in Figure 3, since $V_{Average}$ = 2.72 V, C_{NaCrO_2} = 91.5 mAh (g-$NaCrO_2$)$^{-1}$ and C_{HC} = 226 mAh (g-HC)$^{-1}$, the gravimetric energy density, $W_{Full\text{-}cell}$, is calculated to be 177 Wh (kg-($NaCrO_2$ + HC))$^{-1}$.

Table S4 compares the energy density obtained in this study with those of previously reported sodium-ion full cells. It should be noted that the reported energy densities are calculated based on the weight of the active materials, and that these calculations disregard the contribution of other components such as the conductive agent, binder, current collector, separator, electrolyte, and outer battery case. Moreover, the loading mass of the active material is one of the most important factors to determine the energy density of batteries. There are many full-cell studies of NIBs; some reports have used lower loading mass than that for practical batteries.[12,13,21] Some groups have assembled full cells after eliminating the irreversible capacities of hard carbon negative electrode chemically or electrochemically.[12,21] Dugas *et al.* constructed sodium-ion full cell by a similar way to the present study, and reported the energy density of a HC/$Na_3V_2(PO_4)_2F_3$ full-cell in an organic solvent-based electrolyte to be 237 Wh (kg-($Na_3V_2(PO_4)_2F_3$ + HC))$^{-1}$.[11] Although this value is larger than the value obtained in

the present study, the difference is mainly originated from the average operating potential of positive electrodes. The average operating potentials of $NaCrO_2$ and $Na_3V_2(PO_4)_2F_3$ are 3.0 V and 3.9 V (vs. Na^+/Na), respectively. Assuming that $NaCrO_2$ and $Na_3V_2(PO_4)_2F_3$ positive electrodes show the same capacity in the ionic liquid electrolyte and the operating potential of HC negative electrode is 0.30 V (vs. Na^+/Na), the estimated energy density of the full cell is calculated to be 234 Wh $(kg\text{-}(Na_3V_2(PO_4)_2F_3+HC))^{-1}$ (= 177 × (3.9 − 0.30) / 2.72). Thus, by selecting superior active materials, there is much room to enhance the energy density of the full cell utilizing ionic liquid electrolyte. In our previous NIB full-cell study, loading masses of 5.2 (mg-HC) cm^{-2} and 13.5 (mg-$NaCrO_2$) cm^{-2} realized a gravimetric energy density of 75 Wh kg^{-1} for a 27 Ah-class battery, which corresponds to that of LIBs in the early 2000s.[28] Thus, the results of previous full-cell studies with lower loading masses do not necessarily reflect the performance of practical batteries. Since we utilized high loading masses of 4.8–6.9 (mg-HC) cm^{-2} and 12.3–15.4 (mg-$NaCrO_2$) cm^{-2}, the performance of our full cells is representative of practical batteries. In addition, the cycleability of HC/$NaCrO_2$ full cell is confirmed using the same electrolyte composition. As shown in Figure S3, the discharge capacity and coulombic efficiency in the 1st cycle were 88 mAh $(g\text{-}NaCrO_2)^{-1}$ and 95.6%, respectively. The coulombic efficiency after the 2nd cycle is over 99.5%, and the discharge capacity at the 100th cycle is 79 mAh $(g\text{-}NaCrO_2)^{-1}$, which corresponds to 90% capacity retention.

3.3 Rate capabilities of the HC/$NaCrO_2$ full cells with different sodium-ion concentrations

Figure 4 shows the discharge curves of HC/$NaCrO_2$ full cells with *x*(Na[FSA]) =

0.20 and 0.40 at different discharge rates. The charge rate is fixed at 0.5C, and the discharge rates are varied from 0.5C to 8C. For *x*(Na[FSA]) = 0.20 (Figure 4a), a discharge capacity of 89 mAh $(g\text{-}NaCrO_2)^{-1}$ is obtained at 1C rate, which corresponds to 97% of the capacity at 0.5C rate. However, the capacity falls to 52 mAh $(g\text{-}NaCrO_2)^{-1}$ at 2C rate, and further decreases to less than 20 mAh $(g\text{-}NaCrO_2)^{-1}$ at 4C and 8C rates. On the other hand, when the sodium salt composition is increased to *x*(Na[FSA]) = 0.40 (Figure 4b), improved rate performance is observed. A discharge capacity of 79 mAh $(g\text{-}NaCrO_2)^{-1}$ is maintained at 2C rate, which is 1.5 times as great as the capacity in the case of *x*(Na[FSA]) = 0.20. When the discharge curves at 2C rate are compared, almost no differences are observed in the potential profiles of the HC negative electrodes (dotted lines). On the other hand, the potential profiles of the $NaCrO_2$ positive electrodes (broken lines) are different, *i.e.*, the potential rapidly drops at a capacity of 50 mAh $(g\text{-}NaCrO_2)^{-1}$ for *x*(Na[FSA]) = 0.20. Since the sodium insertion reaction occurs at the positive electrode during the discharge process, the sodium-ion concentration decreases in the electrolyte inside the $NaCrO_2$ composite electrode. The potential drop is thus explained by the depletion of sodium ions in the electrode. In the case of *x*(Na[FSA]) = 0.40, such sodium-ion depletion is less likely to occur than the case of *x*(Na[FSA]) = 0.20, which results in a higher discharge capacity. In other words, electrolytes with higher sodium-ion concentrations have a superior sodium-ion supplying capability. In fact, we reported a similar improvement in the discharge rate capability of a $NaCrO_2$ electrode using $Na/NaCrO_2$ half cells at 363 K.[29] The discharge rate capabilities for the compositions of *x*(Na[FSA]) = 0.30 and 0.50 are also evaluated, as shown in Figure S4.

Figure 5 shows the rate dependence of the discharge capacity at *x*(Na[FSA]) = 0.20–

0.50. Discharge capacities of approximately 90 mAh $(g\text{-}NaCrO_2)^{-1}$ are obtained at 0.5C rate. For electrolytes with sodium-ion concentrations higher than x(Na[FSA]) = 0.30, the capacities are maintained at around 80 mAh $(g\text{-}NaCrO_2)^{-1}$ at 2C rate. The concentration dependence becomes distinct at discharge rates higher than 4C. Larger discharge capacities are observed for highly concentrated electrolytes, especially for the composition of x(Na[FSA]) = 0.50, in which 84% of the capacity is retained even at 4C rate.

Figure 6 compares the charge curves of the HC/$NaCrO_2$ full cells for the electrolyte compositions of x(Na[FSA]) = 0.20 and 0.40. The discharge rate is fixed at 0.5C, and the charge rates are varied from 0.5C to 8C. The charge capacities decreased with increasing charge rates for both compositions. A significant difference in the charge curves is observed at 2C rate. As shown in Figure 6a, for x(Na[FSA]) = 0.20, the charge capacity decreases to 37 mAh $(g\text{-}NaCrO_2)^{-1}$ at 2C rate. On the other hand, a charge capacity of 67 mAh $(g\text{-}NaCrO_2)^{-1}$ is retained at 2C rate for x(Na[FSA]) = 0.40 (Figure 6b). When the charge curves at 2C rate are compared for the two compositions, no notable differences are observed in the potential profiles of the $NaCrO_2$ positive electrodes (broken lines). However, for x(Na[FSA]) = 0.20, the potential of the HC negative electrode (dotted lines) rapidly decreases and reaches the cut-off potential (0.002 V vs. Na^+/Na), leading to lower charge capacity. Since the sodium insertion reaction occurs at the negative electrode during the charge process, the supply of the sodium ion in the HC negative electrode determines the rate capability of full-cell charging. The charge rate capability for x(Na[FSA]) = 0.30 and 0.50 are shown in Figure S5.

Figure 7 summarizes the charge rate capability of the HC/$NaCrO_2$ full cells. Charge

capacities over 90 mAh (g-$NaCrO_2$)$^{-1}$ are observed at 0.5C rate, except for the composition *x*(Na[FSA]) = 0.30. As in the discharge rate capability tests, a clear difference is observed at 2C rate. Higher capacity retention is achieved with increasing sodium-ion concentration in the electrolyte. The capacity at 8C rate in the electrolyte *x*(Na[FSA]) = 0.30 falls to nearly zero. Based on the charge curve, unexpected deterioration may have occurred mainly in the $NaCrO_2$ positive electrode (Figure S5a). However, the overall performance depends on the sodium-ion supplying capability in the electrolytes inside the composite electrodes.

4. Conclusions

We investigated the performance of HC/$NaCrO_2$ full cells in Na[FSA]–[C_3C_1pyrr][FSA] ionic liquid electrolytes with various sodium-ion concentrations (*x*(Na[FSA]) = 0.20–0.50) at 333 K. In particular, to evaluate the performance of practical sodium-ion batteries, we utilized electrodes with high loading masses of 4.8–6.9 (mg-HC) cm^{-2} and 12.3–15.4 (mg-$NaCrO_2$) cm^{-2}. First, via half-cell tests, we determined the practical capacities of HC and $NaCrO_2$ to be 250 mAh (g-HC)$^{-1}$ and 115 mAh (g-$NaCrO_2$)$^{-1}$, respectively. The HC/$NaCrO_2$ full cell exhibited a reversible capacity of 92 mAh (g-$NaCrO_2$)$^{-1}$, resulting in an energy density of 177 Wh (kg-($NaCrO_2$ + HC))$^{-1}$. We evaluated the effect of the sodium-ion concentration on the rate capability of the HC/$NaCrO_2$ full cells by utilizing three-electrode cells, and discussed its mechanism based on the potential profiles of the positive and negative electrodes. In the discharge process, better rate capability was obtained using electrolytes with higher sodium-ion concentrations at discharge rates over 2C. Since the potential profiles of the $NaCrO_2$ positive electrodes were different during the discharge

process, the sodium-ion supplying capability of the electrolyte inside the composite electrodes determines the full-cell capacity. Similar behavior was observed for the charge rate capability tests, *i.e.*, a steep decrease in the potential of the HC negative electrodes reduced the full-cell capacity for lower sodium electrolyte compositions. This phenomenon was also interpreted in terms of sodium-ion depletion in the electrolyte inside the composite electrode during the sodium insertion reaction. In conclusion, ionic liquid with concentrated sodium ion will realize high-power sodium-ion batteries.

Acknowledgments

This study was partly supported by the Advanced Low Carbon Technology Research and Development Program (ALCA) of Japan Science and Technology Agency (JST), and MEXT program "Elements Strategy Initiative to Form Core Research Center" (since 2012), MEXT; Ministry of Education Culture, Sports, Science and Technology, Japan.

References

1. J.M. Tarascon and M. Armand, *Nature*, **414**, 359 (2001).
2. P.V. Braun, J. Cho, J.H. Pikul, W.P. King, and H. Zhang, *Curr. Opin. Solid State Mat. Sci.*, **6**, 186 (2012).
3. H. Matsumoto, H. Sakaebe, K. Tatsumi, M. Kikuta, E. Ishiko, and M. Kono, *J. Power Sources*, **160**, 1308 (2006).
4. M. Ishikawa, T. Sugimoto, M. Kikuta, E. Ishiko, and M. Kono, *J. Power Sources*, **162**, 658 (2006).
5. A. Guerfi, S. Duchesne, Y. Kobayashi, A. Vijh, and K. Zaghib, *J. Power Sources*,

175, 866 (2008).

6. N. Yabuuchi, K. Kubota, M. Dahbi, and S. Komaba, *Chem. Rev.*, **114**, 11636 (2014).
7. D. Larcher and J.M. Tarascon, *Nat. Chem.*, **7**, 19 (2015).
8. M.I. Jamesh and A.S. Prakash, *J. Power Sources*, **378**, 268 (2018).
9. S.R. Taylor and S.M. McLennan, *The Continental Crust: its Composition and Evolution*, Blackwell Scientific Publication, Oxford, UK (1985).
10. M.S. Quinby-Hunt and K.K. Turehian, *EOS*, **64**, 130 (1983).
11. R. Dugas, B. Zhang, P. Rozier, and J.M. Tarascon, *J. Electrochem. Soc.*, **163**, A867 (2016).
12. M. Keller, C. Vaalma, D. Buchholz, and S. Passerini, *ChemElectroChem*, **3**, 1124 (2016).
13. X. Li, P. Yan, M.H. Engelhard, A.J. Crawford, V.V. Viswanathan, C. Wang, J. Liu, and V.L. Sprenkle, *Nano Energy*, **27**, 664 (2016).
14. S.A.M. Noor, P.C. Howlett, D.R. MacFarlane, and M. Forsyth, *Electrochim. Acta*, **114**, 766 (2013).
15. D. Monti, E. Jónsson, M.R. Palacín, and P. Johansson, *J. Power Sources*, **245**, 630 (2014).
16. H. Yoon, H. Zhu, A. Hervault, M. Armand, D.R. MacFarlane, and M. Forsyth, *Phys. Chem. Chem. Phys.*, **16**, 12350 (2014).
17. L.G. Chagas, D. Buchholz, L. Wu, B. Vortmann, and S. Passerini, *J. Power Sources*, **247**, 377 (2014).
18. M. Forsyth, H. Yoon, F. Chen, H. Zhu, D.R. MacFarlane, M. Armand, and P.C. Howlett, *J. Phys. Chem. C*, **120**, 4276 (2016)

19. T. Carstens, A. Lahiri, N. Borisenko, and F. Endres, *J. Phys. Chem. C*, **120**, 14736 (2016)
20. I. Hasa, S. Passerini, and J. Hassoun, *J. Power Sources*, **303**, 203 (2016).
21. C.V. Manohar, T.C. Mendes, M. Kar, D. Wang, C. Xiao, M. Forsyth, S. Mitra, and D.R. MacFarlane, *Chem. Commun.*, **54**, 3500 (2018).
22. K. Kubota, T. Nohira, and R. Hagiwara, *J. Chem. Eng. Data*, **55**, 3142 (2010).
23. A. Fukunaga, T. Nohira, Y. Kozawa, R. Hagiwara, S. Sakai, K. Nitta, and S. Inazawa, *J. Power Sources*, **209**, 52 (2012).
24. K. Matsumoto, Y. Okamoto, T. Nohira, and R. Hagiwara, *J. Phys. Chem. C*, **119**, 7648 (2015).
25. C. Ding, T. Nohira, K. Kuroda, R. Hagiwara, A. Fukunaga, S. Sakai, K. Nitta, and S. Inazawa, *J. Power Sources*, **238**, 296 (2013).
26. C.Y. Chen, K. Matsumoto, T. Nohira, C. Ding, T. Yamamoto, and R. Hagiwara, *Electrochim. Acta*, **133**, 583 (2014).
27. T. Yamamoto, T. Yamaguchi, T. Nohira, R. Hagiwara, A. Fukunaga, S. Sakai, and K. Nitta, *Electrochemistry*, **85**, 391 (2017).
28. A. Fukunaga, T. Nohira, R. Hagiwara, K. Numata, E. Itani, S. Sakai, and K. Nitta, *J. Appl. Electrochem.*, **46**, 487 (2016).
29. C. Ding, T. Nohira, R. Hagiwara, K. Matsumoto, Y. Okamoto, A. Fukunaga, S. Sakai, K. Nitta, and S. Inazawa, *J. Power Sources*, **269**, 124 (2014).
30. C. Ding, T. Nohira, A. Fukunaga, and R. Hagiwara, *Electrochemistry*, **83**, 91 (2015).
31. T. Yamamoto, K. Matsumoto, R. Hagiwara, and T. Nohira, *J. Phys. Chem. C*, **121**, 18450 (2017).

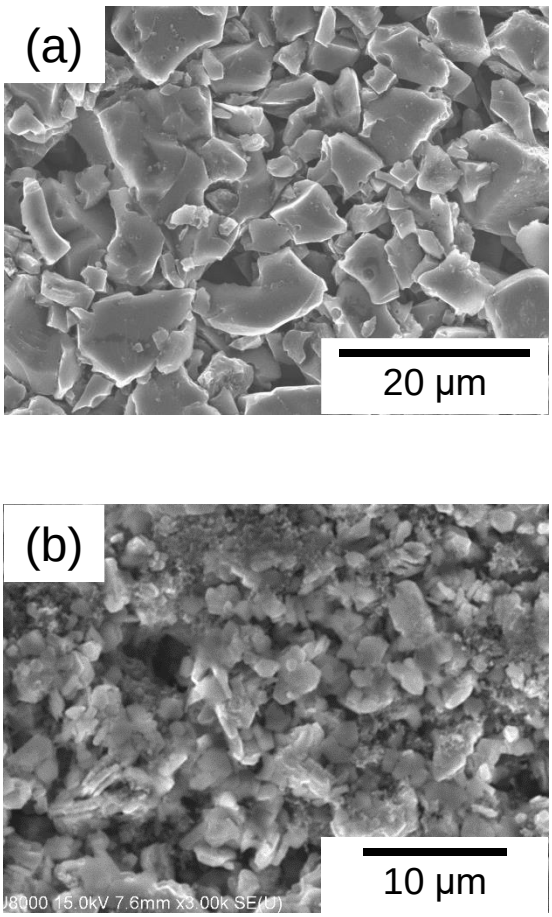

Figure 1 Representative surface SEM images of hard carbon (**a**) and $NaCrO_2$ (**b**) electrodes.

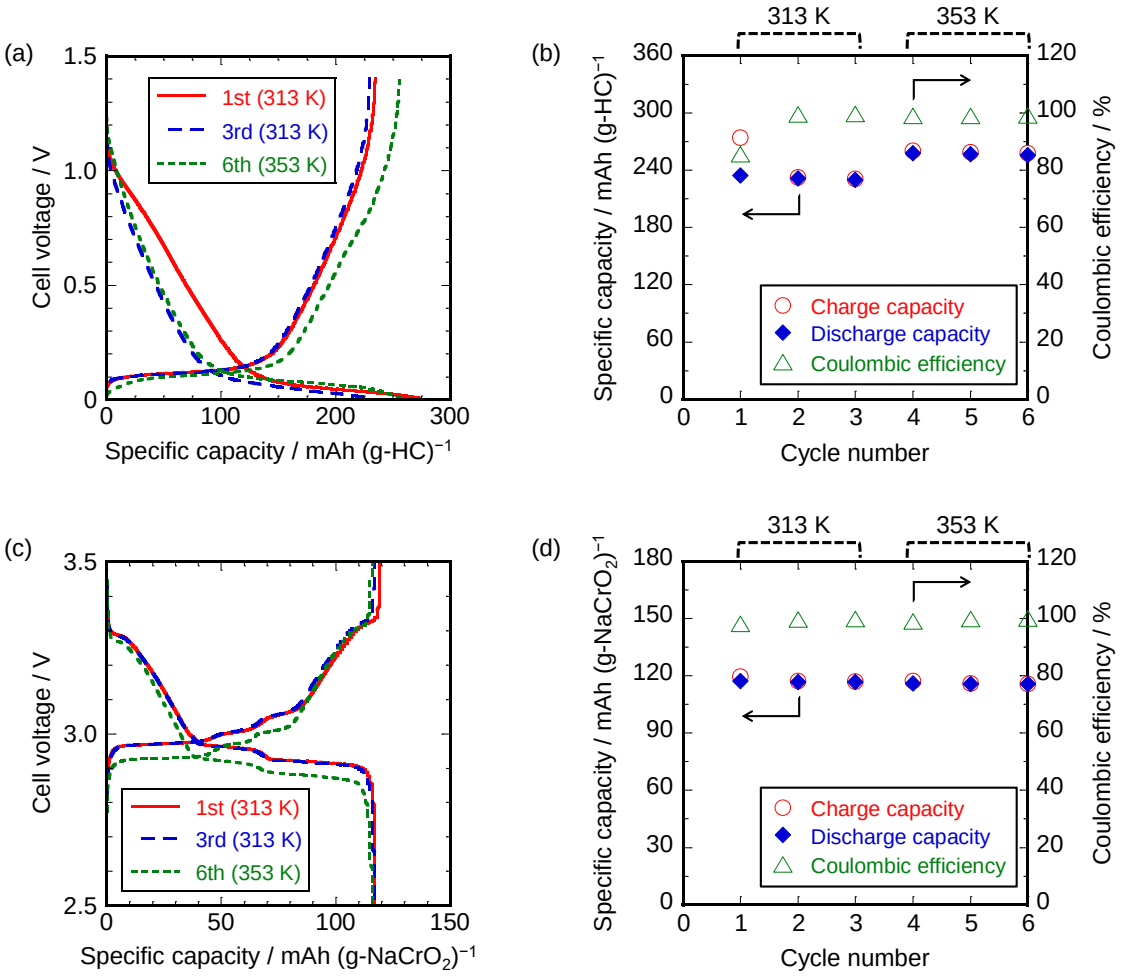

Figure 2 Typical charge–discharge performance of the HC and $NaCrO_2$ electrodes in Na[FSA]–[C_3C_1pyrr][FSA] ionic liquid electrolytes. (**a**) Charge–discharge curves of a Na/Na[FSA]–[C_3C_1pyrr][FSA]/HC half cell (x(Na[FSA]) = 0.20). Charge rate: 25 mA (g-HC)$^{-1}$. Discharge rate: 25 mA (g-HC)$^{-1}$ (1st–3rd cycle) and 125 mA (g-HC)$^{-1}$ (4th–6th cycle). Operating temperature: 313 K (1st–3rd cycle) and 353 K (4th–6th cycle). (**b**) Cycling properties of specific capacity and coulombic efficiency of the Na/HC half-cell. (**c**) Charge–discharge curves of a Na/Na[FSA]–[C_3C_1pyrr][FSA]/$NaCrO_2$ half-cell (x(Na[FSA]) = 0.20). Charge rate: 10 mA (g-$NaCrO_2$)$^{-1}$. Discharge rate: 10 mA (g-$NaCrO_2$)$^{-1}$ (1st–3rd cycle) and 50 mA (g-$NaCrO_2$)$^{-1}$ (4th–6th cycle). Operating temperature: 313 K (1st–3rd cycle) and 353 K (4th–6th cycle). (**d**) Cycling properties of specific capacity and coulombic efficiency of the Na/$NaCrO_2$ half-cell.

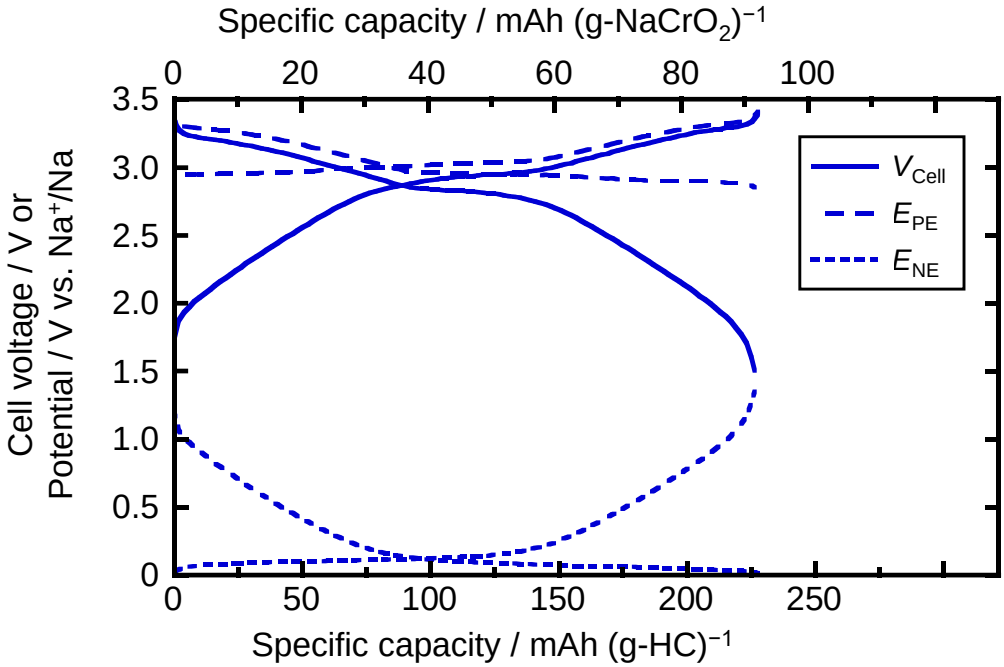

Figure 3 Charge–discharge curves of a HC/Na[FSA]–[C_3C_1pyrr][FSA]/$NaCrO_2$ full-cell (x(Na[FSA]) = 0.20). Operating temperature: 333 K. Charge–discharge rate: 0.5C (1C = 100 mA $(g\text{-}NaCrO_2)^{-1}$). The legends, V_{Cell}, E_{PE}, and E_{NE} are the cell voltage, the potential of the $NaCrO_2$ positive electrode and the potential of the HC negative electrode, respectively.

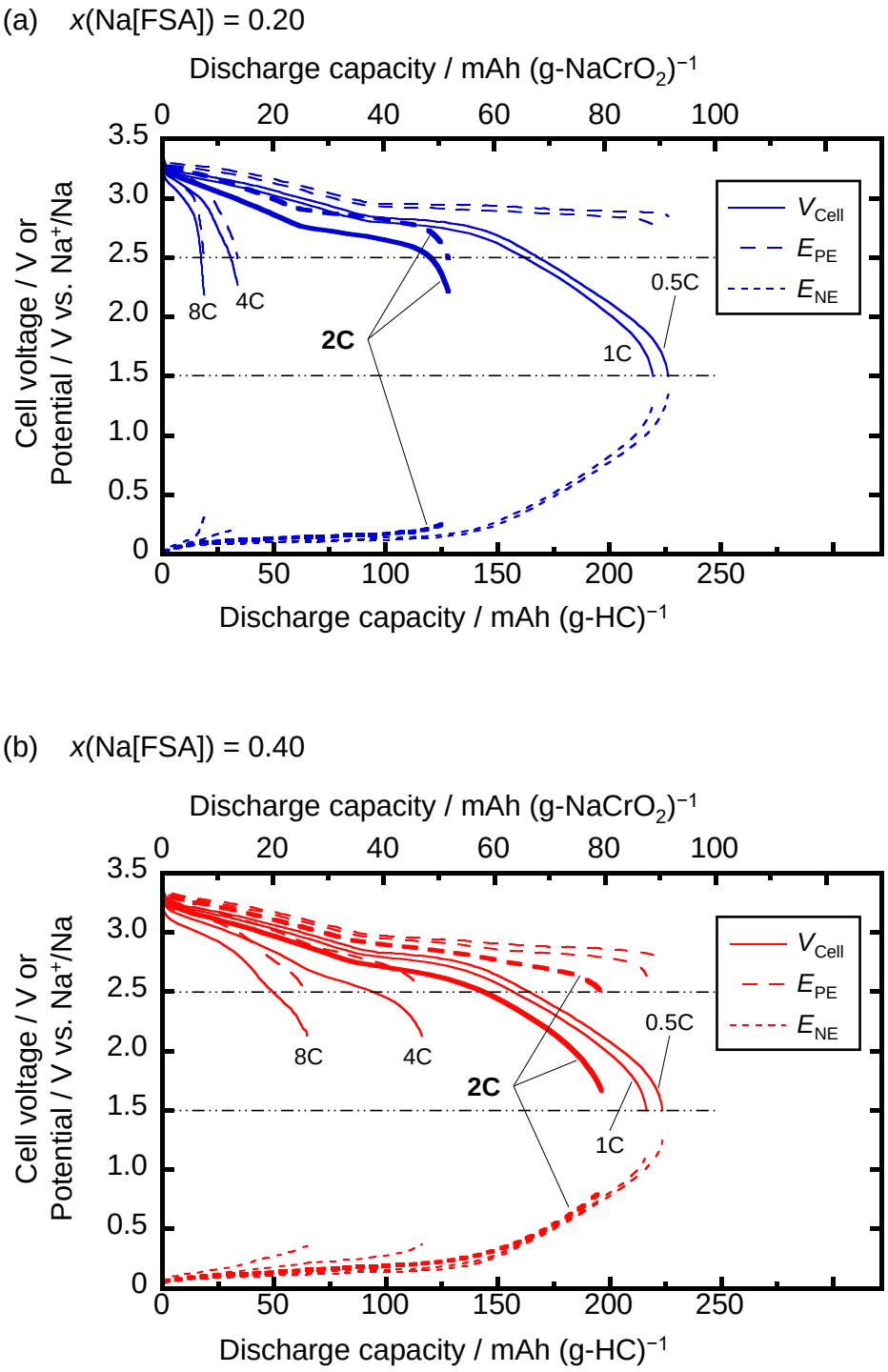

Figure 4 Discharge curves of the HC/Na[FSA]–[C_3C_1pyrr][FSA]/$NaCrO_2$ full-cells at 333 K. Charge rate: 0.5C. Discharge rates: 0.5–8C (1C = 100 mA (g-$NaCrO_2$)$^{-1}$). (**a**) Discharge curves for *x*(Na[FSA]) = 0.20. (**b**) Discharge curves for *x*(Na[FSA]) = 0.40.

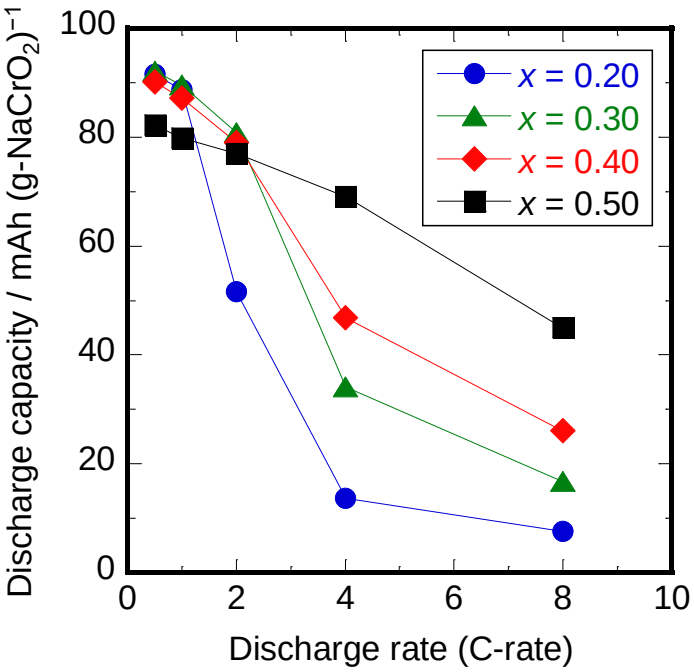

Figure 5 Rate dependence of discharge capacity for the HC/Na[FSA]–[C_3C_1pyrr][FSA]/$NaCrO_2$ full-cells (x(Na[FSA]) = 0.20–0.50) at 333 K. Charge rate: 0.5C. Discharge rates: 0.5–8C (1C = 100 mA $(g\text{-}NaCrO_2)^{-1}$).

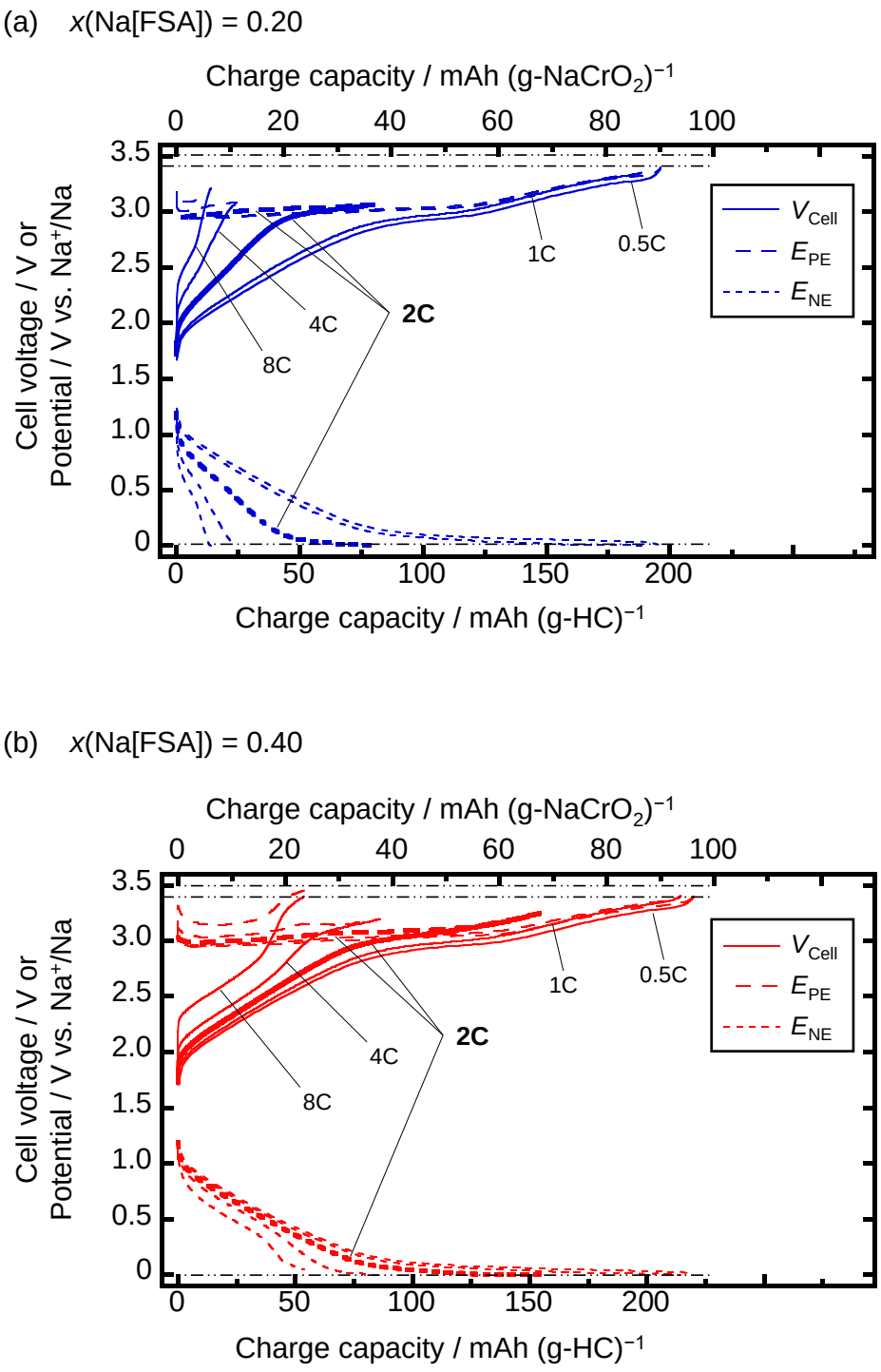

Figure 6 Charge curves of the HC/Na[FSA]–[C_3C_1pyrr][FSA]/$NaCrO_2$ full-cells at 333 K. Charge rate: 0.5–8C. Discharge rates: 0.5C (1C = 100 mA (g-$NaCrO_2$)$^{-1}$). (**a**) Charge curves for *x*(Na[FSA]) = 0.20. (**b**) Charge curves for *x*(Na[FSA]) = 0.40.

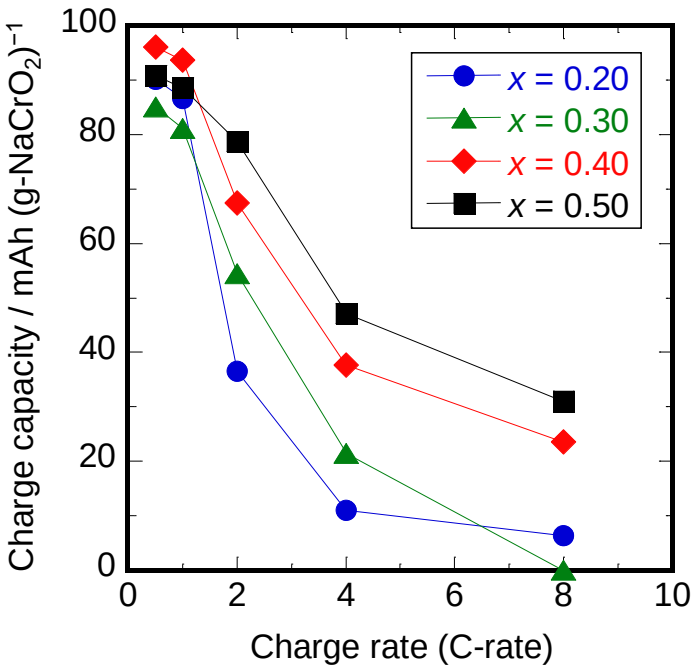

Figure 7 Rate dependence of charge capacity for the HC/Na[FSA]–[C_3C_1pyrr][FSA]/$NaCrO_2$ full-cells (x(Na[FSA]) = 0.20–0.50) at 333 K. Charge rates: 0.5–8C. Discharge rate: 0.5C (1C = 100 mA (g-$NaCrO_2$)$^{-1}$).

Supporting Information

Probing the mechanism of improved performance for sodium-ion batteries by utilizing three-electrode cells: Effects of sodium-ion concentration in ionic liquid electrolytes

Takayuki YAMAMOTO,[1,*] Kazushi MITSUHASHI,[2] Kazuhiko MATSUMOTO,[2] Rika HAGIWARA,[2] Atsushi FUKUNAGA,[3] Shoichiro SAKAI,[3] Koji NITTA,[3] and Toshiyuki NOHIRA[1,*]

[1] Institute of Advanced Energy, Kyoto University, Gokasho, Uji 611-0011, Japan

[2] Graduate School of Energy Science, Kyoto University, Yoshida-honmachi, Sakyo-ku, Kyoto 606-8501, Japan

[3] Sumitomo Electric Industries, Ltd., 1-1-3 Shimaya, Konohana-ku, Osaka 554-0024, Japan

[*] Corresponding Authors:

*E-mail: yamamoto.takayuki.2w@kyoto-u.ac.jp, Tel: +81-774-38-3498, Fax: +81-774-38-3499 (T.Y.).

*E-mail: nohira.toshiyuki.8r@kyoto-u.ac.jp, Tel: +81-774-38-3500, Fax: +81-774-38-3499 (T.N.).

Table S1 Na^+ ion concentrations (mol dm^{-3}) of Na[FSA]–[C_3C_1pyrr][FSA] ionic liquids containing various molar ratios of Na[FSA] at 333 K.*

x(Na[FSA])	0.20	0.30	0.40	0.50
Na^+ ion concentration	1.0	1.5	2.2	3.0

* Calculated from the results of density measurement in the previous report.[24]

Table S2 Loading masses (mg cm^{-2}) of hard carbon (HC) and $NaCrO_2$, and N/P ratios of HC/Na[FSA]–[C_3C_1pyrr][FSA]/$NaCrO_2$ full-cells used for the measurement of discharge rate properties.

		x(Na[FSA])			
		0.20	0.30	0.40	0.50
Loading mass	HC	5.29	5.19	5.08	4.85
	$NaCrO_2$	13.1	12.3	12.6	12.3
N/P ratio*		0.88	0.91	0.88	0.85

* Assumed practical capacities: 250 mAh $(g\text{-HC})^{-1}$ for the negative electrode and 115 mAh $(g\text{-}NaCrO_2)^{-1}$ for the positive electrode.

Table S3 Loading masses (mg cm^{-2}) of hard carbon (HC) and $NaCrO_2$, and N/P ratios of HC/Na[FSA]–[C_3C_1pyrr][FSA]/$NaCrO_2$ full-cells used for the measurement of charge rate properties.

		x(Na[FSA])			
		0.20	0.30	0.40	0.50
Loading mass	HC	6.18	6.00	6.00	6.81
	$NaCrO_2$	13.4	14.5	13.7	15.4
N/P ratio*		1.00	0.90	0.95	0.96

* Assumed practical capacities: 250 mAh $(g\text{-HC})^{-1}$ for the negative electrode and 115 mAh $(g\text{-}NaCrO_2)^{-1}$ for the positive electrode.

Table S4 Comparison of energy densities of sodium-ion full-cells among previous studies and this study.

Positive electrode (Loading mass)	Negative electrode (Loading mass)	Electrolyte	Energy density / Wh kg^{-1}	Remarks**	Ref.
$NaCrO_2$ (12.3–15.4 mg cm^{-2})	HC (4.8–6.9 mg cm^{-2})	1.0–3.0 mol dm^{-3} Na[FSA]–[C_3C_1pyrr][FSA]	177		This study
$Na_3V_2(PO_4)_2F_3$ (ca. 14 mg cm^{-2})	HC (ca. 5 mg cm^{-2})	1 mol dm^{-3} $NaPF_6$ in EC–DMC	237		11
$Na_{0.76}Mn_{0.5}Ni_{0.3}Fe_{0.1}Mg_{0.1}O_2$ (2.73 mg cm^{-2})	HC (1.19 mg cm^{-2})	1 mol dm^{-3} $NaPF_6$ in PC	243	Irreversible capacity of NE was eliminated by pretreatment.	12
$Na_{0.44}MnO_2$ (ca. 2 mg cm^{-2})	HC (ca. 2 mg cm^{-2})	1 mol dm^{-3} $NaClO_4$ in EC–DMC	(313)*		13
$Na_3V_2(PO_4)_3$ (Unknown)	HC (Unknown)	1 mol dm^{-3} Na[FSA]–[C_3C_1pyrr][FSA]	(368)*	Irreversible capacity of NE was eliminated by pretreatment.	21

*Energy density was calculated by using only the weight of the positive active material.
**NE = Negative electrode

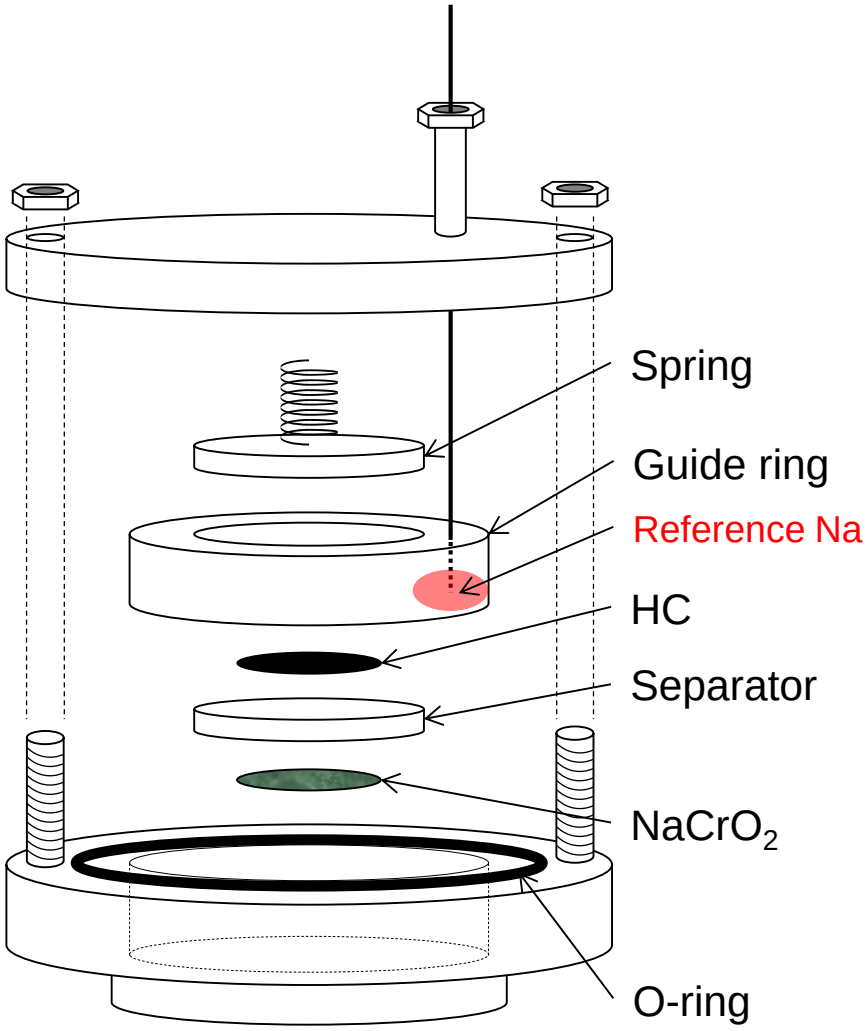

Figure S1 A schematic drawing of the three-electrode cell for charge–discharge tests of HC/$NaCrO_2$ full cells.

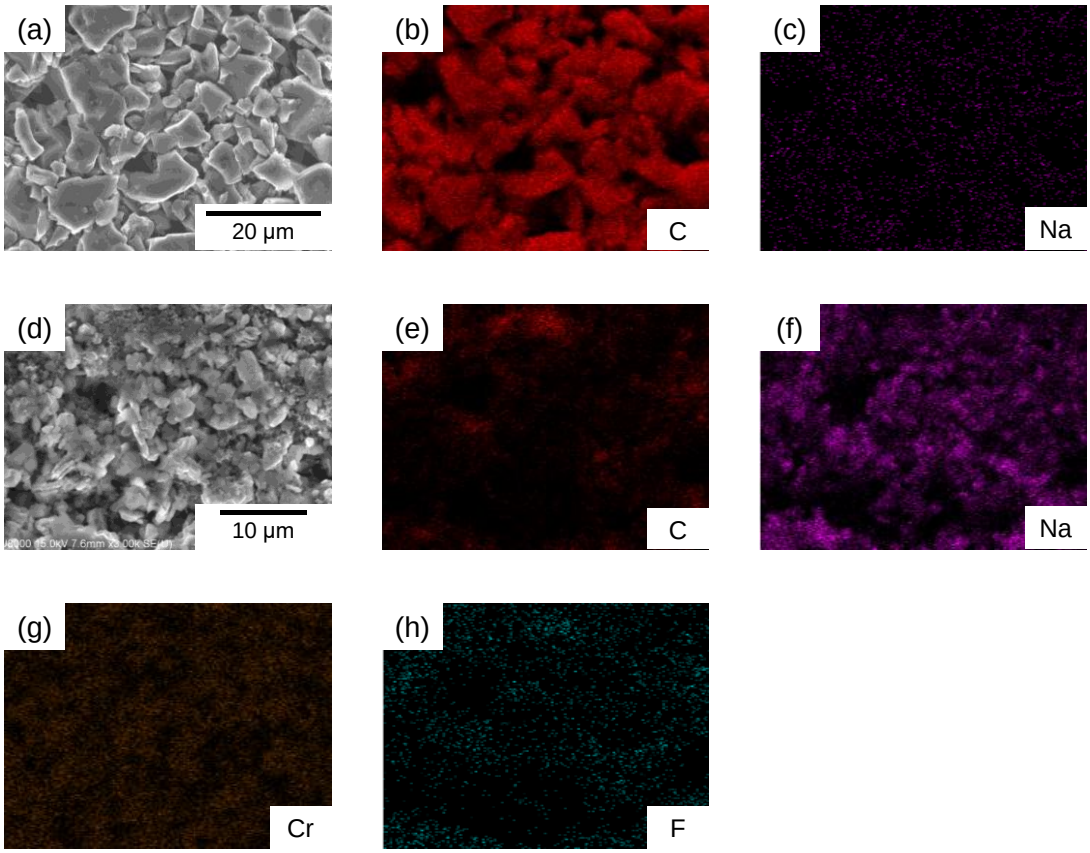

Figure S2 Representative surface SEM and EDX mapping of pristine hard carbon (**a–c**) and $NaCrO_2$ (**d–h**) electrodes.

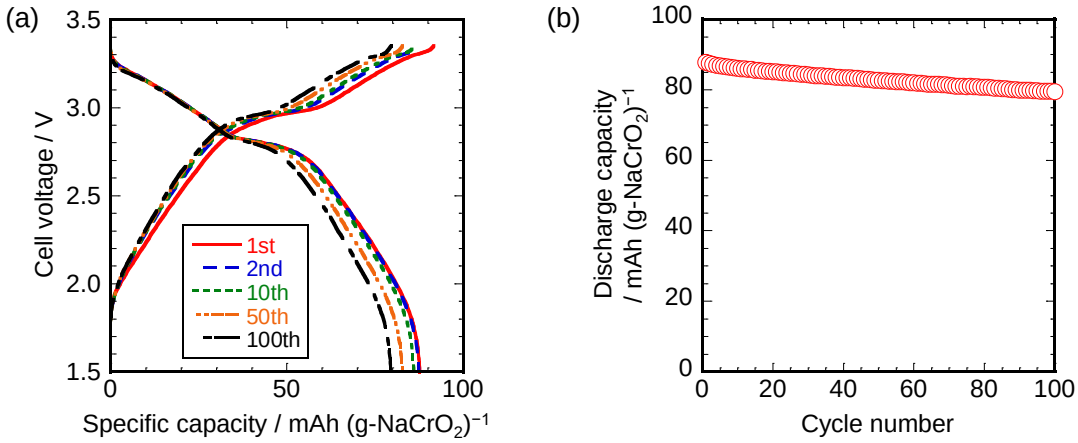

Figure S3 (**a**) Charge–discharge curves and (**b**) cycling properties of specific capacity and coulombic efficiency of the HC/Na[FSA]–[C_3C_1pyrr][FSA]/$NaCrO_2$ (*x*(Na[FSA]) = 0.20) full cell (2032-type coin cell). Charge–discharge rate: 0.5C (= 50 mA (g-$NaCrO_2$)$^{-1}$). Cut-off voltages: 3.35 and 1.50 V. Operating temperature: 333 K. Loading masses: 6.19 mg cm^{-2} (HC) and 15.1 mg cm^{-2} ($NaCrO_2$).

(a) x(Na[FSA]) = 0.30

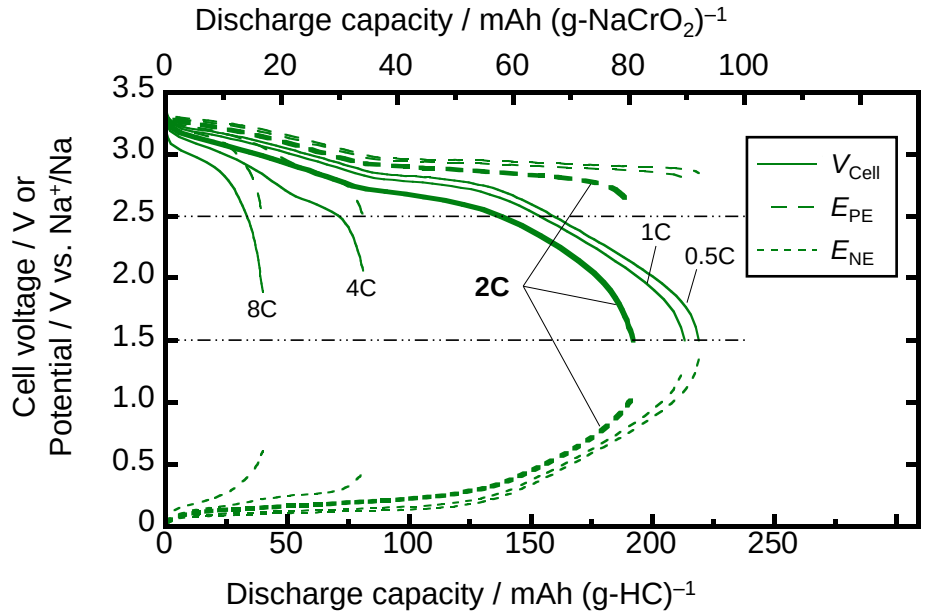

(b) x(Na[FSA]) = 0.50

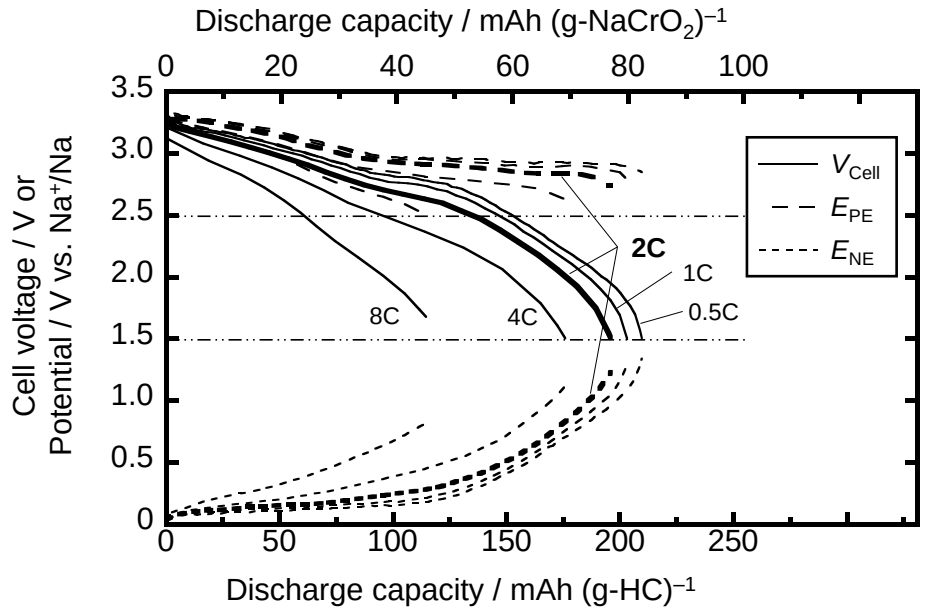

Figure S4 Discharge curves of the HC/Na[FSA]–[C_3C_1pyrr][FSA]/$NaCrO_2$ full-cells at 333 K. Charge rate: 0.5C. Discharge rates: 0.5–8C (1C = 100 mA $(g\text{-}NaCrO_2)^{-1}$). (**a**) Discharge curves for x(Na[FSA]) = 0.30. (**b**) Discharge curves for x(Na[FSA]) = 0.50.

(a) x(Na[FSA]) = 0.30

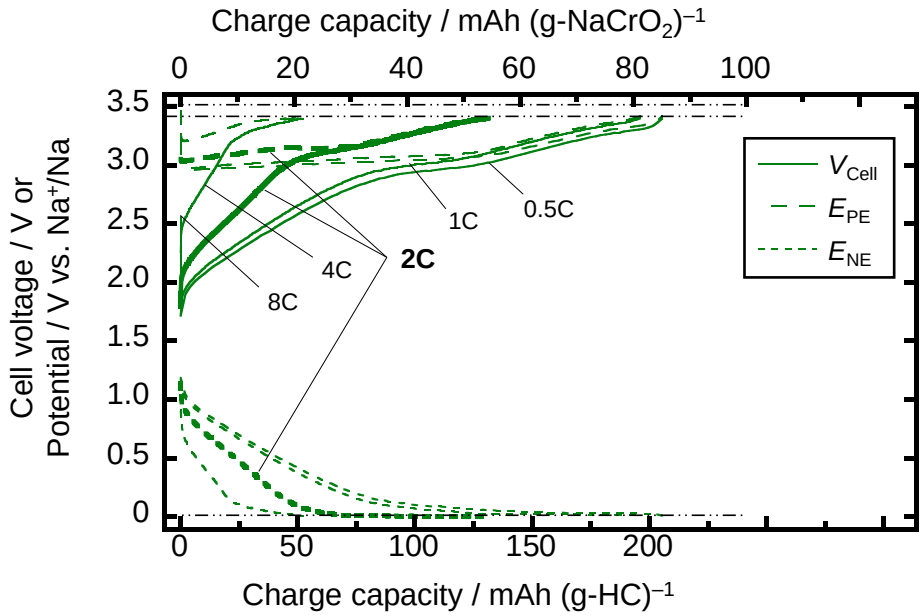

(b) x(Na[FSA]) = 0.50

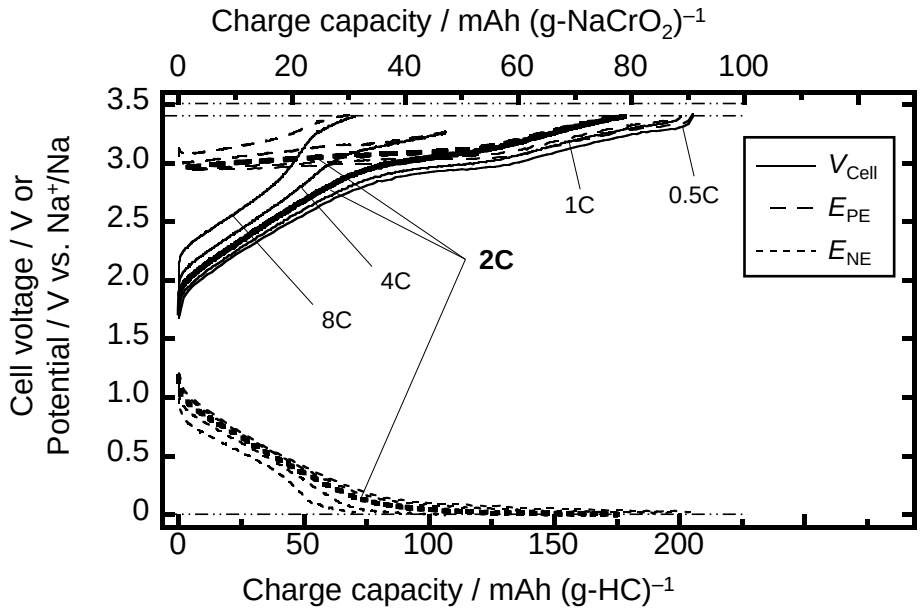

Figure S5 Charge curves of the HC/Na[FSA]–[C_3C_1pyrr][FSA]/$NaCrO_2$ full-cells at 333 K. Charge rate: 0.5–8C. Discharge rates: 0.5C (1C = 100 mA (g-$NaCrO_2$)$^{-1}$). (**a**) Charge curves for x(Na[FSA]) = 0.30. (**b**) Charge curves for x(Na[FSA]) = 0.50.